# Parameter Estimation of Fluctuating Two-Ray Model for Next Generation Mobile Communications

Bo Shi, Luca Pallotta, *Senior Member, IEEE*, Gaetano Giunta, *Senior Member, IEEE*, Chengpeng Hao, *Senior Member, IEEE*, and Danilo Orlando, *Senior Member, IEEE*

***Abstract*—This paper focuses on the problem of parameter estimation for a Fluctuating Two-Ray (FTR) model in the context of wireless mobile communications. Precisely, the received signal is assumed to be the superposition of two dominant components (typically a direct plus a reflected path signal) in addition to diffusive secondary contributions. The signal components may be affected by random amplitude shadowing, statistically modeled by Nakagami-$m$ distribution, multiplied by unknown scaling factors with random uniform independent phases, whereas the diffusive component is assumed to follow the complex Gaussian distribution. Exploiting the method of moments, a $4\times4$ nonlinear system is herein mathematically derived, which is very hard to be solved due to the strong nonlinearity. Therefore, a sequential procedure based on some prior information about the diffusive component power level is devised to solve it. The effectiveness of the proposed estimation technique is shown by evaluating the normalized root mean square errors as well as mean errors and standard deviations in several operating conditions of practical interest also considering the limit case of only one-ray in order to compare the proposed approach to simpler estimators, already presented in the literature. The results show the robustness of the new estimator even under a multipath model mismatch. Finally, the effectiveness of the proposed estimation procedure is confirmed through measured mmWave data.**

***Keywords*—Two-ray model, 5G, Nakagami-$m$ distribution, method of moments, statistical estimators, mmWave.**

## I. Introduction

Future generation wireless networks are aimed at spreading the available spectrum resources to provide users and connected objects with an increased speed, bandwidth, and capacity. In particular, the Internet of Things (IoT) is expected to massively expand the use of 5G networks, that are continuously evolving to meet the requirements of future applications related to cellular operations, IoT security, and network challenges [1]. 5G-based communications will be capable to connect diverse IoT devices which may be deployed in wide geographical ranges leading to heterogeneous communication scenarios. So far, the Nakagami-$m$ fading model [2] is a prominent candidate to cover all the possible scenarios for future broadband wireless communication system, since it is suitable for the characterization of a class of channels that is wider than that associated to Rayleigh and Rician fading [3]. To this end the millimeter wave (mmWave), i.e., between 30 and 300 GHz, and device-to-device (D2D) are regarded as promising technologies [4]–[9]. As a matter of fact, in the last years, they experienced a wide growth due to the increasing demand in cellular channels capacity that requires new technologies as primary solution to contrast a possible congestion of the traffic [10]–[12]. Therefore, many researches have been driven to the design of suitable models for the communication channels related to these novel devices [13]–[15].

In practice, the above mentioned model, sometimes referred to as "Rician shadowed fading" model [16], because it generalizes the Rician fading one, reflects any amplitude fluctuation in the specular waves (e.g., variations in the propagation condition or fast moving scatterers) that takes place over the time period of interest. For completeness, before proceeding further, it is important to recall that, the received signals in wireless communications systems rapidly vary due to the random fluctuations of both phases and amplitudes as well as time of arrival. These fluctuations generates the so-called small-scale fading which is typically described through Rayleigh, Rician, Nakagami-$m$ distributions and others. More precisely, in the absence of a dominant contribution, i.e., in a non-line of sight (NLoS) environment, the widest utilized approximation for the received I-Q signals is the Gaussian distribution, that leads to the Rayleigh one for its envelope (or Exponential for its power). However, in many situations of practical interest, a line of sight (LoS) component, which dominates the weak diffusive contributions, is also present and the received signal envelope for this small-scale fading path amplitudes must be described by other distributions such as, for instance, the Rician distribution [17], [18]. A statistical model, capable of encompassing all the aforementioned situations as special cases, is the Nakagami-$m$ distribution, developed in [2]. In fact, by tuning its shape parameter, $m$ say, it is possible to obtain the Gaussian fading (for $m=1$, the Nakagami-$m$ distribution approximates the Rayleigh distribution) or to model the no fading channel (for $m$ going to infinity) [19]. Moreover, it has been widely demonstrated through experiments and measurements on field, that in many environments, the Nakagami-$m$ distribution has good fits with the fading radio channel from acquired data [19]–[22]. So far, the reviewed fading models do not consider the possible random variations of the LoS components, which can be due to partial block of the LoS due

L. Pallotta and G. Giunta are with the Department of Engineering, University of Roma Tre, via Vito Volterra 62, 00146 Rome, Italy (e-mail: luca.pallotta@uniroma3.it, gaetano.giunta@uniroma3.it).

B. Shi and C. Hao are with the Institute of Acoustics, Chinese Academy of Sciences, Beijing 100190, China (e-mail: tthrx@qq.com, haochengp@mail.ioa.ac.cn).

D. Orlando is with the Faculty of Engineering, Università degli Studi "Niccolò Cusano", Via Don Carlo Gnocchi 3, 00166 Roma, Italy. E-mail: danilo.orlando@unicusano.it.

to the presence of obstacles such as trees, buildings, and so on between the transmitter and receiver device [16]. In order to account for this behavior (therefore reducing model mismatch losses), the shadowed fading model has been introduced. As a matter of fact, in this situation, also the LoS component is a stochastic variable, modeled sometimes as a log-Normal [23], or in most cases with a simpler Nakagami-$m$ random variable [16].

Recently, the Nakagami-$m$ fading model has evolved in the so-called fluctuating two-ray (FTR) fading model, which has been proposed as a versatile model that well characterizes the small-scale fading effects on the wireless propagation in mmWave and D2D environments [5], [24]. In fact, FTR fading model fits well experimental wireless channels, such as outdoor millimeter-wave field measurements at 28 GHz where a bimodality behavior in its empirical probability density function (pdf) has been experienced [24]. Moreover, it also encompasses several well known distributions as, for instance, the Gaussian, Rayleigh, Rician and Nakagami-$m$ ones, as special or limiting cases [25]. Another important feature that has contributed to the introduction of the FTR model in these contexts is that even though it shares a bimodal structure, it can be also seen as a generalization of unimodal Rician, Nakagami-$m$, Rayleigh models and so on [24]–[26]. As a matter of fact, in the absence of a LoS contribution, the FTR becomes the Rayleigh model since only the diffusive Gaussian components are present. On the other hand, if a dominant LoS term is available at the receiver side, it becomes unimodal, such as Rician, Nakagami-$m$ distributions and so on, as well as the corresponding shadowed alternatives in case of amplitude fluctuations. However, especially for mmWave devices widely utilized for short distance links, due to the presence of ground and/or buildings, besides the direct transmitted signal, also the one reflected by these surfaces often impinges on the receiver [7], [27]. Therefore, an FTR model represents a suitable tool to manage the received signal in these contexts. Figure 1 shows a pictorial representation of the above mentioned FTR model highlighting the two dominant signal components acquired at the receiver side.

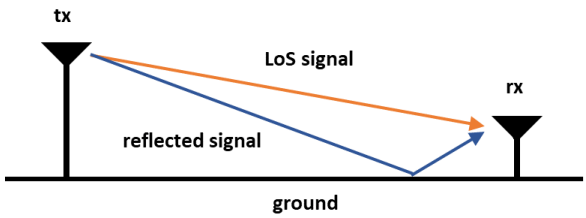


Figure 1. Pictorial representation of the two-ray model.

More precisely, the received signal, when a single ground reflection dominates the multipath effect [28], can be seen as the superposition of the following signals:

- a direct term propagating in free space that is the so-called LoS ray or component[1];
- a second dominant component that is the transmitted signal that undergoes a single reflection on a plane or surface between transmitter and receiver (e.g., reflected by the ground and/or a building, etc.);
- several contributions arising from random backscattering by the objects present in the scene (referred to as diffusive component).

Although the FTR model was also recently studied for applications, such as physical layer security [29] and channel capacity [26], the estimation of FTR model parameters, at least to best of authors' knowledge, has received less attention. For this reason, in this paper, we fill this gap and devise a novel estimation procedure for FTR model parameters. At the design stage, we assume that the two rays undergo the same fluctuation. This assumption naturally raises in different wireless scenarios. In fact, if the scattering centers are located in proximity of the transmitter or receiver, the specular components will travel alongside most of the way and, hence, would share almost the same fluctuations [27]. The proposed algorithm relies on the method of moments [30] which leads to a system of nonlinear expressions obtained by computing four high order moments of the received signal amplitude. Finding closed form expressions for the solution of the considered system is not an easy task due the high level of nonlinearity. For this reason, we resort to a sequential procedure that exploits some a-priori information about the diffusive component. Specifically, starting from a prior estimate of the power level of the diffusive component and after some algebraic manipulations, the quoted system is reduced to a $2 \times 2$ nonlinear system composed by a second- and fourth-order equations. Solving this new system of equations enforcing also some physical constraints on the involved parameters, two unknowns can be found. Then, accounting for the remaining relationships among the unknowns, the others are directly obtained from the former (a point better explained in what follows). The effectiveness of the devised algorithm is evaluated through simulations, using as figure of merit the normalized root mean square error (NRMSE) and the mean estimates of the proposed estimators. The results demonstrate that the proposed approach is able to provide good estimation capabilities in several contexts of practical interest together with a reduced computational burden. Finally, the effectiveness of the proposed strategy is also confirmed by exploiting measured mmWave data.

The paper is organized as follows. Section II formulates the problem, providing the FTR model together with the expression of the four considered high-order moments. Section III describes the proposed parameters estimation procedure based on the method of moments. In Section IV the behavior of the proposed estimation technique is investigated accounting for different situations of practical interest. Finally, Section V concludes the paper and outlines possible future research tracks.

## NOTATION

We adopt the notation of using $\Re\{\cdot\}$, $|\cdot|$, and $(\cdot)^*$ to indicate the real part, the modulus and the complex conjugate of the argument, respectively. The acronym i.i.d. means

[1]Note that, the two-ray model is still valid if in place of the LoS component there is a dominant reflected signal.

independent and identical distributed. $\mathbb{E}[\cdot]$ stands for statistical expectation whereas the letter $j$ indicates the imaginary unit, i.e., $j = \sqrt{-1}$. The gamma function is denoted by $\Gamma(m)$, whereas $\Phi(x, y; a) = {}_1F_1(x; y; a)$ is the Kummer Confluent Hypergeometric Function [31]. We write $x \sim \mathcal{CN}(\mu, \sigma^2)$ if $x$ is a circular complex normal random variable with mean $\mu$ and variance $\sigma^2 > 0$; Finally, $x \sim \mathcal{U}(0, 2\pi)$ means that $x$ obeys the uniform distribution within the interval $[0, 2\pi]$.

## II. Problem Formulation

In this section, the estimation problem for the FTR model parameters is suitably defined [28]. Precisely, the focus is on a generic wireless communication channel characterized by the presence of two dominant components (two-ray) in addition to diffusive secondary paths. According to this model, the complex baseband received signal can be written as

$$z = (v_1 e^{j\varphi_1} + v_2 e^{j\varphi_2}) r + \varepsilon, \tag{1}$$

where:

- $v_i \in \mathbb{R}$, $i = 1, 2$, are unknown deterministic scaling factors accounting for the specific path propagation losses. In the following of this paper, without loss of generality, we are assuming that $v_1$ and $v_2$ are real positive (or null) scaling factors with $v_1 \geq v_2$.
- $\varphi_i$, $i = 1, 2$, are the phases of the complex amplitude of the received component, modeled as independent uniform random variable in the interval $[0, 2\pi]$, i.e., $\varphi_i \sim \mathcal{U}[0, 2\pi]$, $i = 1, 2$.
- $r \in \mathbb{R}^+$ is a random variable representing the shadowing of both the LoS component and the main reflected signal (LoS shadow fading), that derives from the relative motion of the transmitter and receiver pair as well as the possible variability of the scene (e.g., moving cars, oscillating trees due to wind conditions, and so on) that could provide a partial masking of the signal path. It is worth underlining that, following the lead of [24], we assume the same fluctuation phenomena for both the LoS and the reflected component. For instance, when the reflection arises in proximity of either the transmitter or the receiver, it can be claimed that the two dominant components follow approximately the same path, sharing the same fluctuations.
- $\varepsilon = \varepsilon_r - j\varepsilon_i \sim \mathcal{CN}(0, \sigma^2)$ independent of $r$ and $\varphi_i$, $i = 1, 2$. This component is given by the superposition of the thermal noise generated by the electronic devices and the diffusive NLoS paths. Moreover, $\varepsilon_r$ and $\varepsilon_i$ denotes its real and imaginary parts, respectively.

As for the shadow fading factor, it is modeled as a Nakagami-$m$ random variable, since this statistical model better describes most of the fading channels with respect to Rayleigh and Rician distributions. Moreover, the latter can be obtained as special cases of a Nakagami-$m$ distribution [3], [28], [32]. Generally speaking, the pdf of the Nakagami-$m$ distribution is given by [28]

$$p_r(r) = \frac{2m^m r^{2m-1}}{\Gamma(m)\Omega^m} \exp\left[\frac{-mr^2}{\Omega}\right], \quad m \geq 0.5, \tag{2}$$

with $\Omega$ and $m$ the spread and fading (or shape) parameters, respectively. However, since $v_1$, $v_2$, and $\Omega$ are not known, the latter is statistically meaningless. As a matter of fact, given $c \in \mathbb{R}$, $z$ can be expressed as

$$\begin{aligned} z &= c\left(v_1 e^{j\varphi_1} + v_2 e^{j\varphi_2}\right) r/c + \varepsilon \\ &= \left(v_1 c e^{j\varphi_1} + v_2 c e^{j\varphi_2}\right) r/c + \varepsilon \\ &= \left(v_1' e^{j\varphi_1} + v_2' e^{j\varphi_2}\right) r_1 + \varepsilon, \end{aligned} \tag{3}$$

where $v_1'$ and $v_2'$ are unknown, whereas $r_1$ follows the Nakagami distribution with parameters $m$ and $\Omega/c^2$. Thus, the likelihood function of $z$ takes on the same value when computed at $(v_1, v_2, \Omega, m)$ and $(v_1', v_2', \Omega/c^2, m)$. Otherwise stated, the considered parameter models for $z$ are not identifiable [33], [34]. For this reason and without loss of generality, we can set $\Omega = 1$ (namely, $c = \Omega$) leaving $v_1$ and $v_2$ unaltered. Therefore, the Nakagami-$m$ moments simplify as

$$\begin{cases} \mathbb{E}[|r|^2] = 1 \\ \mathbb{E}[|r|^4] = \dfrac{m+1}{m} \\ \mathbb{E}[|r|^6] = \dfrac{(m+1)(m+2)}{m^2} \\ \mathbb{E}[|r|^8] = \dfrac{(m+1)(m+2)(m+3)}{m^3} \end{cases} \tag{4}$$

As already claimed, the aim of this paper is to provide a procedure towards the estimation of the unknown parameters $v_1$, $v_2$, $m$, and $\sigma^2$. To this end, we compute the expressions of the first four even noncentral moments of $z$.
As a preliminary step, let us first explicitly write the square modulus of the received signal

$$\begin{aligned} |z|^2 &= zz^* \\ &= \left[v_1^2 + v_2^2 + 2v_1 v_2 \cos(\varphi_1 - \varphi_2)\right] r^2 + |\varepsilon|^2 \\ &+ 2(v_1 \cos\varphi_1 + v_2 \cos\varphi_2)\varepsilon_r r \\ &+ 2(v_1 \sin\varphi_1 + v_2 \sin\varphi_2)\varepsilon_i r. \end{aligned} \tag{5}$$

Now, exploiting the independence among the involved random variables, it is possible to derive the first four even moments of $z$, viz. $|z|^{2n}$, $n = 1, \ldots, 4$. Precisely, the second and fourth moment can be easily derived as

$$\mu_2 = \mathbb{E}[|z|^2] = v_1^2 + v_2^2 + \sigma^2, \tag{6}$$

and

$$\begin{aligned} \mu_4 = \mathbb{E}[|z|^4] &= \left(v_1^4 + v_2^4 + 4v_1^2 v_2^2\right) \frac{m+1}{m} \\ &+ 2\sigma^4 + 2\left(v_1^2 + v_2^2\right)\sigma^2 + 2\left(v_1^2 + v_2^2\right)\sigma^2 \\ &= \left[(v_1^2 + v_2^2)^2 + 2v_1^2 v_2^2\right] \frac{m+1}{m} \\ &+ 4(v_1^2 + v_2^2)\sigma^2 + 2\sigma^4. \end{aligned} \tag{7}$$

As for the last two considered moments, in Appendix A we derive their final expressions to come up with the following system of equations

$$\begin{cases} \mu_2 = v_1^2 + v_2^2 + \sigma^2 \\ \mu_4 = \left[(v_1^2+v_2^2)^2 + 2v_1^2v_2^2\right]\dfrac{m+1}{m} + 4(v_1^2+v_2^2)\sigma^2 + 2\sigma^4 \\ \mu_6 = \left[(v_1^2+v_2^2)^3 + 6(v_1^2+v_2^2)v_1^2v_2^2\right]\dfrac{(m+1)(m+2)}{m^2} \\ \quad + 9\left[(v_1^2+v_2^2)^2 + 2v_1^2v_2^2\right]\sigma^2\dfrac{m+1}{m} \\ \quad + 18(v_1^2+v_2^2)\sigma^4 + 6\sigma^6 \\ \mu_8 = \left[(v_1^2+v_2^2)^4 + 6v_1^4v_2^4 + 12(v_1^2+v_2^2)^2v_1^2v_2^2\right] \\ \quad \times \dfrac{(m+1)(m+2)(m+3)}{m^3} \\ \quad + \left[16(v_1^2+v_2^2)^2 + 96v_1^2v_2^2\right](v_1^2+v_2^2)\sigma^2\dfrac{(m+1)(m+2)}{m^2} \\ \quad + \left[72(v_1^2+v_2^2)^2 + 144v_1^2v_2^2\right]\sigma^4\dfrac{m+1}{m} \\ \quad + 96(v_1^2+v_2^2)\sigma^6 + 24\sigma^8 \end{cases} \tag{8}$$

In the next section, we devise a procedure to find a solution of the above system.

## III. Parameters Estimation Procedure

This section is aimed at finding a procedure to properly estimate the model parameters $(v_1, v_2, m, \sigma^2)$ involved in the system (8). Precisely, the parameters estimation procedure devised in this paper is based on the method of moments [30] and can be synthetically described through the following guidelines:

1) introducing the change of variables $x_1 = v_1^2 + v_2^2$, $x_2 = v_1^2v_2^2$, $x_3 = \frac{1}{m}$, $x_4 = \sigma^2$, the system of equation given in (8) can be transformed in a novel system in the variables $x_i$, $i = 1, \ldots, 4$;
2) starting from the moments estimates, say $\hat{\mu}_2, \hat{\mu}_4, \hat{\mu}_6, \hat{\mu}_8$, and exploiting some prior knowledge about $x_4$, the devised system of equations is sequentially solved providing the corresponding values of $x_1$, $x_2$, $x_3$, and $x_4$.
3) from the estimates of the unknown $x_1$, $x_2$, $x_3$, and $x_4$, those of the physical parameters, viz. $v_1$, $v_2$, $m$, and $\sigma^2$, are derived. In all cases, the multiplicity of the solutions is reduced by the physical constraints of powers $(v_1^2, v_2^2, \sigma^2)$ and of the parameter $m$ of Nakagami-$m$ distribution which must be positive (and integer) as well as exploiting the likelihood of the received signal reported in Appendix B.

Given the above, the system of equations in the new variables $x_i$, $i = 1, \ldots, 4$ is given by

$$\mu_2 = x_1 + x_4 \tag{9}$$

$$\mu_4 = (x_1^2 + 2x_2)(1 + x_3) + 4x_1x_4 + 2x_4^2 \tag{10}$$

$$\begin{aligned} \mu_6 &= (x_1^2 + 6x_2)x_1(1 + x_3)(1 + 2x_3) \\ &\quad + (9x_1^2 + 18x_2)x_4(1 + x_3) \\ &\quad + 18x_1x_4^2 + 6x_4^3 \end{aligned} \tag{11}$$

$$\begin{aligned} \mu_8 &= (x_1^4 + 6x_2^2 + 12x_1^2x_2) \\ &\quad \times (1 + x_3)(1 + 2x_3)(1 + 3x_3) \\ &\quad + (16x_1^2 + 96x_2)x_1x_4(1 + x_3)(1 + 2x_3) \\ &\quad + (72x_1^2 + 144x_2)x_4^2(1 + x_3) \\ &\quad + 96x_1x_4^3 + 24x_4^4 \end{aligned} \tag{12}$$

It is now worth underlining that the system of equations (9)-(12) is a nonlinear system. As a consequence, a direct solution of the system with $4$ unknowns is not possible because the equation set is highly nonlinear. Of course, a possible procedure for solving the quoted non-linear system of equations could consist in the direct application of the Levenberg-Marquardt algorithm [35], [36]. Precisely, the Levenberg-Marquardt algorithm (LMA) solves the generic problem $F(\boldsymbol{x}) = \mathbf{0}$ made of non-linear equations and vectorial unknowns by iterative local linearization of the equations. However, the LMA converges towards the optimum solution only if the initial working point of $\boldsymbol{x}^{(0)}$ is in a "close" neighborhood of that solution. For these reasons, in what follows we devise a strategy aimed at directly solving the system at hand.

### A. Method of Moments based Procedure

To search for one (or more) solutions for the system (9)-(12), we can firstly solve (9) for $x_4$, and substitute it in the remaining equations. However, before doing this, we introduce the actual estimates of all the considered moments obtained as the sample moments, i.e.,

$$\begin{cases} \hat{\mu}_2 = \dfrac{1}{N}\displaystyle\sum_{i=1}^{N}|z_i|^2 \\ \hat{\mu}_4 = \dfrac{1}{N}\displaystyle\sum_{i=1}^{N}|z_i|^4 \\ \hat{\mu}_6 = \dfrac{1}{N}\displaystyle\sum_{i=1}^{N}|z_i|^6 \\ \hat{\mu}_8 = \dfrac{1}{N}\displaystyle\sum_{i=1}^{N}|z_i|^8 \end{cases} \tag{13}$$

with $z_i$, $i = 1, \ldots, N$, denoting samples containing both dominant and diffuse signal components. This choice is motivated by the fact that exploiting the Kintchine's Strong Law of Large Numbers [37] the estimators in (13) are asymptotically unbiased.

Thus, solving (9) with respect to $x_4$ yields

$$x_4 = \hat{\mu}_2 - x_1. \tag{14}$$

Replacing $x_4$ in (10)-(12) with the above expression and exploiting the sample moments in (13), we come up with the following $3\times 3$ system of equations in the three unknowns $x_1$, $x_2$, and $x_3$

$$\begin{cases} \hat{\mu}_4 = (x_1^2+2x_2)(1+x_3) \\ \quad + 4x_1\left(\hat{\mu}_2 - x_1\right) + 2\left(\hat{\mu}_2 - x_1\right)^2 & (15) \\ \hat{\mu}_6 = (x_1^2+6x_2)x_1(1+x_3)(1+2x_3) \\ \quad + 9(x_1^2+2x_2)\left(\hat{\mu}_2 - x_1\right)(1+x_3) \\ \quad + 18x_1\left(\hat{\mu}_2 - x_1\right)^2 + 6\left(\hat{\mu}_2 - x_1\right)^3 & (16) \\ \hat{\mu}_8 = (x_1^4+6x_2^2+12x_1^2x_2) \\ \quad \times (1+x_3)(1+2x_3)(1+3x_3) \\ \quad + (16x_1^2+96x_2)x_1\left(\hat{\mu}_2 - x_1\right)(1+x_3)(1+2x_3) \\ \quad + (72x_1^2+144x_2)\left(\hat{\mu}_2 - x_1\right)^2(1+x_3) \\ \quad + 96x_1\left(\hat{\mu}_2 - x_1\right)^3 + 24\left(\hat{\mu}_2 - x_1\right)^4. & (17) \end{cases}$$

Now, (15) can be rearranged as follows

$$(x_1^2+2x_2)(1+x_3) = \hat{\mu}_4 - 4x_1(\hat{\mu}_2 - x_1) - 2(\hat{\mu}_2 - x_1)^2, \quad (18)$$

that is equivalent to

$$\begin{aligned}(x_1^2+2x_2) + (x_1^2+2x_2)x_3 \\ = \hat{\mu}_4 - 4x_1(\hat{\mu}_2 - x_1) - 2(\hat{\mu}_2 - x_1)^2,\end{aligned} \quad (19)$$

and hence

$$\begin{aligned}(x_1^2+2x_2)x_3 \\ = \hat{\mu}_4 - 4x_1(\hat{\mu}_2 - x_1) - 2(\hat{\mu}_2 - x_1)^2 - (x_1^2+2x_2).\end{aligned} \quad (20)$$

Following the same approach as for (20), namely, multiplying (15) by 2 and solving for $(x_1^2+2x_2)(1+2x_3)$ and multiplying (15) by 3 and solving for $(x_1^2+2x_2)(1+3x_3)$, it is possible to write the following two equalities:

$$\begin{aligned}(x_1^2+2x_2)(1+2x_3) \\ = \hat{\mu}_4 - 4x_1(\hat{\mu}_2 - x_1) - 2(\hat{\mu}_2 - x_1)^2 + \hat{\mu}_4 \\ - 4x_1(\hat{\mu}_2 - x_1) - 2(\hat{\mu}_2 - x_1)^2 - (x_1^2+2x_2)\end{aligned} \quad (21)$$

and

$$\begin{aligned}(x_1^2+2x_2)(1+3x_3) \\ = \hat{\mu}_4 - 4x_1(\hat{\mu}_2 - x_1) - 2(\hat{\mu}_2 - x_1)^2 - (x_1^2+2x_2) \\ + \hat{\mu}_4 - 4x_1(\hat{\mu}_2 - x_1) - 2(\hat{\mu}_2 - x_1)^2 + \hat{\mu}_4 \\ - 4x_1(\hat{\mu}_2 - x_1) - 2(\hat{\mu}_2 - x_1)^2 - (x_1^2+2x_2).\end{aligned} \quad (22)$$

Exploiting (20), (21), and (22), equation(16) can be written in terms of the two unknowns $x_1$ and $x_2$ i.e.

$$\begin{aligned}(x_1^2+2x_2)(x_1^2+2x_2)\hat{\mu}_6 \\ = (x_1^2+6x_2)x_1\left[\hat{\mu}_4 - 4x_1(\hat{\mu}_2 - x_1) - 2(\hat{\mu}_2 - x_1)^2\right] \\ \times \left[\hat{\mu}_4 - 4x_1(\hat{\mu}_2 - x_1) - 2(\hat{\mu}_2 - x_1)^2 + \hat{\mu}_4\right. \\ \left. -4x_1(\hat{\mu}_2 - x_1) - 2(\hat{\mu}_2 - x_1)^2 - (x_1^2+2x_2)\right] \\ + (x_1^2+2x_2)9(x_1^2+2x_2)(\hat{\mu}_2 - x_1) \\ \times \left[\hat{\mu}_4 - 4x_1(\hat{\mu}_2 - x_1) - 2(\hat{\mu}_2 - x_1)^2\right] \\ + (x_1^2+2x_2)(x_1^2+2x_2)18x_1(\hat{\mu}_2 - x_1)^2 \\ + (x_1^2+2x_2)(x_1^2+2x_2)6(\hat{\mu}_2 - x_1)^3.\end{aligned} \quad (23)$$

After some algebraic manipulations (i.e., performing all the multiplications in (23) and ordering the resulting terms in decreasing powers of $x_1$), the latter can be recast as

$$\begin{aligned}&\left[4\hat{\mu}_2^2 - 2\hat{\mu}_4 + 8x_2\right]x_1^5 \\ &+ \left[-12\hat{\mu}_2^3 + 9\hat{\mu}_4\hat{\mu}_2 - \hat{\mu}_6\right]x_1^4 \\ &+ \left[8\hat{\mu}_2^4 - 8\hat{\mu}_2^2\hat{\mu}_4 - 8\hat{\mu}_2^2x_2 + 2\hat{\mu}_4^2 + 4\hat{\mu}_4x_2 - 48x_2^2\right]x_1^3 \\ &+ \left[-48x_2\hat{\mu}_2^3 + 36\hat{\mu}_4x_2\hat{\mu}_2 - 4\hat{\mu}_6x_2\right]x_1^2 \\ &+ \left[48\hat{\mu}_2^4x_2 - 48\hat{\mu}_2^2\hat{\mu}_4x_2 + 96\hat{\mu}_2^2x_2^2 + 12\hat{\mu}_4^2x_2 - 48\hat{\mu}_4x_2^2\right]x_1 \\ &- 48\hat{\mu}_2^3x_2^2 + 36\hat{\mu}_4\hat{\mu}_2x_2^2 - 4\hat{\mu}_6x_2^2 = 0\end{aligned} \quad (24)$$

that is a fifth-order equation in $x_1$. Nevertheless, (24) can be also seen as a second-order equation with respect to the unknown $x_2$. Therefore, reorganizing (24) in decreasing order with respect to the powers of $x_2$, it becomes

$$\begin{aligned}&\left[-48\hat{\mu}_2^3 + 96\hat{\mu}_2^2x_1 + 36\hat{\mu}_4\hat{\mu}_2 - 48x_1^3 - 48\hat{\mu}_4x_1 - 4\hat{\mu}_6\right]x_2^2 \\ &+ \left[48\hat{\mu}_2^4x_1 - 48\hat{\mu}_2^3x_1^2 - 48\hat{\mu}_2^2\hat{\mu}_4x_1 - 8\hat{\mu}_2^2x_1^3 + 36\hat{\mu}_2\hat{\mu}_4x_1^2\right. \\ &\left.+12\hat{\mu}_4^2x_1 + 4\hat{\mu}_4x_1^3 + 8x_1^5 - 4\hat{\mu}_6x_1^2\right]x_2 + 8\hat{\mu}_2^4x_1^3 \\ &- 12\hat{\mu}_2^3x_1^4 - 8\hat{\mu}_2^2\hat{\mu}_4x_1^3 + 4\hat{\mu}_2^2x_1^5 + 9\hat{\mu}_2\hat{\mu}_4x_1^4 \\ &+ 2\hat{\mu}_4^2x_1^3 - 2\hat{\mu}_4x_1^5 - \hat{\mu}_6x_1^4 = 0\end{aligned} \quad (25)$$

Exploiting (20), (21), and (22), equation (17) can be also written in terms of only the two unknowns $x_1$ and $x_2$, i.e.,

$$
\begin{aligned}
&(x_1^2+2x_2)(x_1^2+2x_2)(x_1^2+2x_2)\hat{\mu}_8\\
&\quad=(x_1^4+6x_2^2+12x_1^2x_2)\\
&\quad\times\left[\hat{\mu}_4-4x_1(\hat{\mu}_2-x_1)-2(\hat{\mu}_2-x_1)^2\right]\\
&\quad\times\left[\hat{\mu}_4-4x_1(\hat{\mu}_2-x_1)-2(\hat{\mu}_2-x_1)^2+\hat{\mu}_4\right.\\
&\quad\left.-4x_1(\hat{\mu}_2-x_1)-2(\hat{\mu}_2-x_1)^2-(x_1^2+2x_2)\right]\\
&\quad\times\left[\hat{\mu}_4-4x_1(\hat{\mu}_2-x_1)-2(\hat{\mu}_2-x_1)^2-(x_1^2+2x_2)\right.\\
&\quad+\hat{\mu}_4-4x_1(\hat{\mu}_2-x_1)-2(\hat{\mu}_2-x_1)^2+\hat{\mu}_4\\
&\quad\left.-4x_1(\hat{\mu}_2-x_1)-2(\hat{\mu}_2-x_1)^2-(x_1^2+2x_2)\right]\\
&\quad+(x_1^2+2x_2)(16x_1^2+96x_2)x_1(\hat{\mu}_2-x_1)\\
&\quad\times\left[\hat{\mu}_4-4x_1(\hat{\mu}_2-x_1)-2(\hat{\mu}_2-x_1)^2\right]\\
&\quad\times\left[\hat{\mu}_4-4x_1(\hat{\mu}_2-x_1)-2(\hat{\mu}_2-x_1)^2+\hat{\mu}_4\right.\\
&\quad\left.-4x_1(\hat{\mu}_2-x_1)-2(\hat{\mu}_2-x_1)^2-(x_1^2+2x_2)\right]\\
&\quad+(x_1^2+2x_2)(x_1^2+2x_2)(72x_1^2+144x_2)(\hat{\mu}_2-x_1)^2\\
&\quad\times\left[\hat{\mu}_4-4x_1(\hat{\mu}_2-x_1)-2(\hat{\mu}_2-x_1)^2\right]\\
&\quad+(x_1^2+2x_2)(x_1^2+2x_2)(x_1^2+2x_2)96x_1\\
&\quad\times(\hat{\mu}_2-x_1)^3+(x_1^2+2x_2)(x_1^2+2x_2)(x_1^2+2x_2)\\
&\quad\times24(\hat{\mu}_2-x_1)^4.
\end{aligned}
\tag{26}
$$

Equation (26) can be suitably recast following the same line of reasoning as (23). Thus, it becomes

$$
\begin{aligned}
&\left[-96\hat{\mu}_2^2+96x_1^2+48\hat{\mu}_4\right]x_2^4\\
&+\left[-1296\hat{\mu}_2^4+3072\hat{\mu}_2^3x_1+912\hat{\mu}_2^2\hat{\mu}_4-1536\hat{\mu}_2^2x_1^2\right.\\
&-1536\hat{\mu}_2\hat{\mu}_4x_1-1536\hat{\mu}_2x_1^3-84\hat{\mu}_4^2+768\hat{\mu}_4x_1^2\\
&\left.+1296x_1^4-8\hat{\mu}_8\right]x_2^3\\
&+\left[-288\hat{\mu}_2^6+1536\hat{\mu}_2^5x_1+432\hat{\mu}_2^4\hat{\mu}_4-2952\hat{\mu}_2^4x_1^2\right.\\
&-1536\hat{\mu}_2^3\hat{\mu}_4x_1+1280\hat{\mu}_2^3x_1^3-216\hat{\mu}_2^2\hat{\mu}_4^2+2376\hat{\mu}_2^2\hat{\mu}_4x_1^2\\
&+1032\hat{\mu}_2^2x_1^4+384\hat{\mu}_2\hat{\mu}_4^2x_1-640\hat{\mu}_2\hat{\mu}_4x_1^3-512\hat{\mu}_2x_1^5\\
&\left.+36\hat{\mu}_4^3-378\hat{\mu}_4^2x_1^2-516\hat{\mu}_4x_1^4-96x_1^6-12\hat{\mu}_8x_1^2\right]x_2^2\\
&+\left[-576\hat{\mu}_2^6x_1^2+1024\hat{\mu}_2^5x_1^3+864\hat{\mu}_2^4\hat{\mu}_4x_1^2-408\hat{\mu}_2^4x_1^4\right.\\
&-1024\hat{\mu}_2^3\hat{\mu}_4x_1^3-432\hat{\mu}_2^2\hat{\mu}_4^2x_1^2+120\hat{\mu}_2^2\hat{\mu}_4x_1^4-144\hat{\mu}_2^2x_1^6\\
&+256\hat{\mu}_2\hat{\mu}_4^2x_1^3+128\hat{\mu}_2x_1^7+72\hat{\mu}_4^3x_1^2+78\hat{\mu}_4^2x_1^4\\
&\left.+72\hat{\mu}_4x_1^6-24x_1^8-6\hat{\mu}_8x_1^4\right]x_2\\
&-48\hat{\mu}_2^6x_1^4+128\hat{\mu}_2^5x_1^5+72\hat{\mu}_2^4\hat{\mu}_4x_1^4-132\hat{\mu}_2^4x_1^6\\
&-128\hat{\mu}_2^3\hat{\mu}_4x_1^5+64\hat{\mu}_2^3x_1^7-36\hat{\mu}_2^2\hat{\mu}_4^2x_1^4+84\hat{\mu}_2^2\hat{\mu}_4x_1^6\\
&-12\hat{\mu}_2^2x_1^8+32\hat{\mu}_2\hat{\mu}_4^2x_1^5-32\hat{\mu}_2\hat{\mu}_4x_1^7+6\hat{\mu}_4^3x_1^4\\
&-3\hat{\mu}_4^2x_1^6+6\hat{\mu}_4x_1^8-\hat{\mu}_8x_1^6=0
\end{aligned}
\tag{27}
$$

Now, focus on the two-equation system consisting of (25) and (27), and assume that a-priori information about $x_4$ is somehow available at the receiver (for instance, past estimates of the same channel and/or off-line estimation of diffuse component)[2]. Then, an estimate of $x_1$ can be obtained as

$$
\hat{x}_1=\hat{\mu}_2-\hat{x}_4^{(0)},
\tag{28}
$$

where $\hat{x}_4^{(0)}$ is an existing estimate of $x_4$.

Now, for the considered value of $x_1$, both equations (25) and (27) can be solved to obtain at most 2 solutions from the former, say $\hat{x}_2^{(a,1)}$ and $\hat{x}_2^{(a,2)}$, and 4 solutions from the latter, say $\hat{x}_2^{(b,1)}$, $\hat{x}_2^{(b,2)}$, $\hat{x}_2^{(b,3)}$ and $\hat{x}_2^{(b,4)}$. Discarding those solutions which are not real and positive, the remaining are selected as candidates to estimate the model parameters. Since both (25) and (27) must be simultaneously valid, among the possible candidate solutions $\left(\hat{x}_2^{(a,1)},\hat{x}_2^{(a,2)},\hat{x}_2^{(b,1)},\hat{x}_2^{(b,2)},\hat{x}_2^{(b,3)},\hat{x}_2^{(b,4)}\right)$, we must choose a pair of candidates that are ideally identical or, at least, very close each other (in fact, both equations must be satisfied at the same time). To this end, a selection criterion can be the following

$$
\begin{aligned}
\left(\hat{x}_2^{(a)},\hat{x}_2^{(b)}\right)=\arg\min_{\left\{\hat{x}_2^{(a,i)},\hat{x}_2^{(b,k)}\right\}}&\left(\hat{x}_2^{(a,i)}-\hat{x}_2^{(b,k)}\right)^2,\\
&i=1,2,\ k=1,\ldots,4.
\end{aligned}
\tag{29}
$$

Clearly, as a particular case, if no acceptable pair of solutions satisfies the constraints' check, the procedure is aborted, and it should restart with new acquired data. Once the best couple of solutions has been found, its numerical average is utilized as final estimate of $x_2$, i.e.,

$$
\hat{x}_2=\frac{\hat{x}_2^{(a)}+\hat{x}_2^{(b)}}{2}.
\tag{30}
$$

It is worth noticing that $\hat{x}_2$ can be also selected among $\left(\hat{x}_2^{(a)},\hat{x}_2^{(b)}\right)$ as the one that maximizes the likelihood function of the received signal $z$, whose expression is derived in Appendix B (in particular, the considered solutions are used to compute the parameter values used in the likelihood function given $z$, then it is selected the solution returning the highest likelihood value). However, in the simulation conducted in this paper the first approach has been utilized to obtain the final estimate of $x_2$, since several tests have shown the same results in applying the two selection approaches. As the last step, exploiting $\hat{x}_1$, an estimate of $x_4$ can be easily derived from (14), whereas, an estimate of $x_3$ can be estimated from both $\hat{x}_1$ and $\hat{x}_2$ in conjunction with (18), i.e.,

$$
\hat{x}_3=\frac{\hat{\mu}_4-4\hat{x}_1(\hat{\mu}_2-\hat{x}_1)-2(\hat{\mu}_2-\hat{x}_1)^2}{\hat{x}_1^2+2\hat{x}_2}-1.
\tag{31}
$$

[2]Note that, we can reasonably assume that the diffusive component (that includes thermal noise effects) power $\sigma^2$, namely $x_4$, can be a-priori known. If thermal noise is dominant, it can be evaluated characterizing the power level related to the single device components or, at least, using signal free samples acquired from adjacent bandwidths. Conversely, when the noise power level is negligible, the diffusive component can be effectively estimated from previous data blocks in the same bandwidth of interest (also making use of dynamic predictive models). In addition, in a D2D context, close devices could share such information about the channel estimate as well as cooperate to jointly estimate the channel model.

Now, an important remark is given in the following. Precisely, the proposed solution starts with a first knowledge of $x_4$, namely $\hat{x}_4^{(0)}$, whose accuracy directly impact on the estimate of $x_1$ and consequently $x_2$. It is obvious that errors in the estimation of $x_4$ propagates into the other variables estimates, which in some cases could compromise the entire estimation process. To overcome this limitation, a possible solution could consist in defining a reasonable range of search of $x_1$ values, say $[x_{1,\min}, x_{1,\max}]$ centered on $\hat{x}_1$. Then, for each value of $x_1$ belonging to the interval (sampled with a reasonable step) $[x_{1,\min}, x_{1,\max}]$, all the solutions of (25) and (27) are computed. The procedure is applied for each value of $x_1$ and the final pair of $x_2$ estimates, together with the corresponding $\hat{x}_1$ that has generated it, is chosen as the one minimizing (29).

Finally, it is worth to underline that the initial estimate of $x_4$, $\hat{x}_4^{(0)}$, can be obtained resorting to signal free sample acquired before the communication, through the following equation

$$\hat{x}_4^{(0)} = \hat{\mu}_2^{(0)} = \frac{1}{N_0}\sum_{n=1}^{N_0} |z_{0n}|^2. \tag{32}$$

where $z_{0n}$ denotes the $n$-th signal free sample. Algorithm 1 summarizes the main steps of the proposed procedure to find the solution of the problem described by (9)-(12).

**Algorithm 1** Method of Moments based Procedure

1: **Input:** Gaussian samples $z_{0n}$, $n = 1, \ldots, N_0$, and signal plus diffuse component samples $z_i$, $i = 1, \ldots, N$;
2: **Output:** Unknown estimates of the system (9)-(12), $\hat{x}_1$, $\hat{x}_2$, $\hat{x}_3$, and $\hat{x}_4$;
3: Initialization of $x_4$ estimate, i.e., $\hat{x}_4^{(0)} = \hat{\mu}_2^{(0)}$, from Gaussian samples $z_{0n}$ with (32);
4: Moments estimation $\hat{\mu}_2$, $\hat{\mu}_4$, $\hat{\mu}_6$, $\hat{\mu}_8$ from dominant and diffuse signal components samples $z_i$ with (13);
5: $\hat{x}_1$ estimation through (28);
6: Get the roots of (25) and (27), $\left(\hat{x}_2^{(a,1)}, \hat{x}_2^{(a,2)}, \hat{x}_2^{(b,1)}, \hat{x}_2^{(b,2)}, \hat{x}_2^{(b,3)}, \hat{x}_2^{(b,4)}\right)$;
7: Verify the constraints on the obtained solutions;
8: Select the best couple of $x_2$ estimates, $\left(\hat{x}_2^{(a)}, \hat{x}_2^{(b)}\right)$, through (29);
9: Obtain the final estimate of $x_2$, i.e., $\hat{x}_2$ through (30) or maximizing the received signal likelihood;
10: $\hat{x}_3$ and $\hat{x}_4$ evaluation starting from $\hat{x}_1$ and $\hat{x}_2$ exploiting (14) and (31).

### B. Parameter Estimation of Fluctuating Two-Ray Model

Once the system of equations described in (9)-(12) is solved by means of the proposed procedure, the parameter estimation of fluctuating two-ray model can be accomplished. Precisely, starting from the final estimates $\hat{x}_1$, $\hat{x}_2$, $\hat{x}_3$, and $\hat{x}_4$, the parameters $v_1$, $v_2$, $m$, and $\sigma^2$ can be obtained as follows:

- Diffuse signal component $\sigma^2$

$$\hat{\sigma}^2 = \hat{x}_4, \tag{33}$$

- Nakagami-$m$ shape parameter $m$

$$\hat{m} = \frac{1}{\hat{x}_3}, \tag{34}$$

- scaling factor $v_1$ as the solution of the following 2-nd order equation

$$\left(v_1^2\right)^2 - \hat{x}_1 v_1^2 + \hat{x}_2 = 0, \tag{35}$$

namely,

$$\hat{v}_1^2 = \frac{\hat{x}_1 \pm \sqrt{\hat{x}_1^2 - 4\hat{x}_2}}{2} \tag{36}$$

- scaling factor $v_2$

$$\hat{v}_2^2 = \frac{\hat{x}_2}{\hat{v}_1^2}. \tag{37}$$

It is important to observe that, according to (35), there are up to four real solutions for $\hat{v}_1$, say $\hat{v}_a$, $-\hat{v}_a$, $\hat{v}_b$, and $-\hat{v}_b$. It can be easy proven that, due to (37), the (up to) four solutions $\hat{v}_2$ are numerically the same as for $\hat{v}_1$, but switched in their order, viz: $\hat{v}_b$, $-\hat{v}_b$, $\hat{v}_a$, and $-\hat{v}_a$. For sake of simplicity, we have assumed $v_1 \geq v_2$ in the model definition (1) without loss of generality, after taking only the positive (or null) solutions into account. As a consequence, we can consider only one solution for $\hat{v}_1$ and $\hat{v}_2$, with the constraint $\hat{v}_1 \geq \hat{v}_2 \geq 0$, for each pair of values of $\hat{x}_1$ and $\hat{x}_2$.

## IV. Performance Assessment

This section is aimed at analyzing the performance of the proposed method-of-moments-based procedure for the considered FTR model. To this end, the performance metrics are the NRMSE and the mean estimate (ME) of the parameters.

Specifically, indicating with $\hat{y}$ the generic estimate of the generic parameter $y$ (viz. $v_1$, $v_2$, $\sigma^2$, and $m$), the NRMSE and ME are given by

$$\text{NRMSE} = \sqrt{\mathbb{E}\left[\left|1 - \frac{\hat{y}}{y}\right|^2\right]} \tag{38}$$

and

$$\text{ME} = \mathbb{E}\left[\hat{y}\right], \tag{39}$$

respectively. Now, due to the lack of closed-form expressions for the above metrics, we estimate them resorting to $M_C = 1000$ independent Monte Carlo trials, namely

$$\text{NRMSE} = \sqrt{\frac{1}{M_C}\sum_{i=1}^{M_C}\left|1 - \frac{\hat{y}_i}{y}\right|^2} \tag{40}$$

and

$$\text{ME} = \frac{1}{M_C}\sum_{i=1}^{M_C}\hat{y}_i, \tag{41}$$

where $\hat{y}_i$ is the related estimate obtained at the $i$-th trial.

This section comprises two parts. In the first part, the performance of the proposed approach is assessed by resorting to simulated data and under the design assumptions. On the

other hand, the second part is devoted to the analysis on measured mmWave data.

### A. Simulated Data

The NRMSE and the ME are investigated with respect to all the involved parameters, namely:

1) number of samples utilized for the moments estimate;
2) ratio between the average power of the dominant waves and that of the diffuse multipath;
3) ratio between the dominant waves powers;
4) shape parameter of the Nakagami-$m$ distribution.

Finally, a comparison with the parameter estimator devised in [32] for the one-ray Nakagami-$m$ shadowing is also conducted.

In the first analysis, the following simulating scenario is considered. The power of the LoS component is assumed equal to $v_1^2 = 5$ whereas that of the reflected ray is $v_2^2 = 4$, the diffusive component power is instead set equal to $\sigma^2 = 1$ and the fading parameter is set as $m = 5$. Figure 2 shows the RMSE values of the four involved parameter estimates versus the number of samples $N$ utilized to compute the moments, $\mu_2$, $\mu_4$, $\mu_6$, and $\mu_8$.

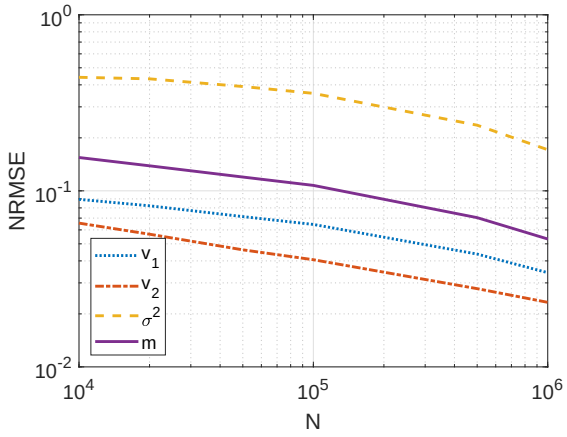


Figure 2. NRMSE versus the number of samples $N$. The considered simulating scenario assumes $v_1^2 = 5$, $v_2^2 = 4$, $\sigma^2 = 1$, and $m = 5$. A total of $M_C = 1000$ Monte Carlo trials are performed.

The curves show that, as expected, the RMSE reduces as the amount of data utilized to evaluate the sample moments increases. In addition, it can be observed from the figure that $\hat{m}$ exhibits the worst error value. This is mainly due to the fact that the parameter $m$ is obtained from the unknown $x_3$ which in turn depends on the estimates of the remaining parameters, therefore it is affected by the error propagation. However, the proposed algorithm is able to reach satisfactory performance for a number of data greater than $10^4$ for all the considered parameters.

Figure 3 reports the ME values of the quoted parameter estimates versus the number of samples $N$ assuming the same parameter setting as in Figure 2. In the figure, the confidence intervals (i.e., ME $\pm$ standard deviation) are plotted too to draw a picture of the dispersion of the estimates around their mean value. In the figure, the true value of the parameter under investigation is indicated with a black dashed curve.

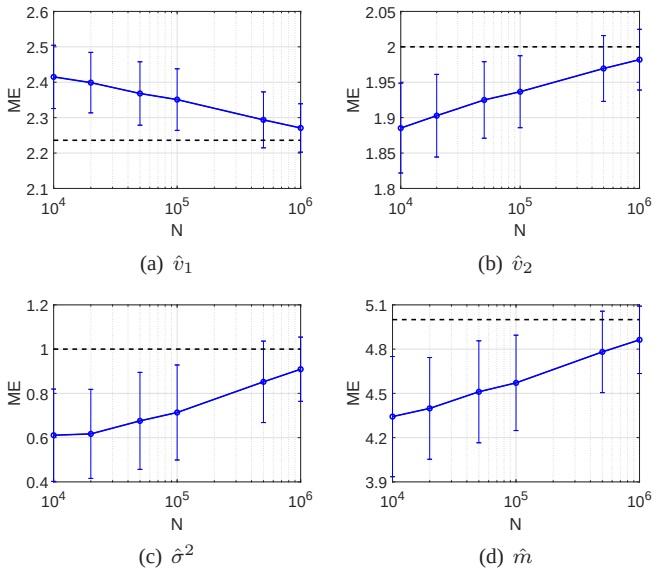


Figure 3. ME with confidence interval versus the number of samples $N$. The considered simulating scenario assumes $v_1^2 = 5$, $v_2^2 = 4$, $\sigma^2 = 1$, and $m = 5$. A total of $M_C = 1000$ Monte Carlo trials are performed. Subplots refers to the estimates a) $\hat{v}_1$, b) $\hat{v}_2$, c) $\hat{\sigma}^2$, and d) $\hat{m}$. Black dashed lines indicate the true parameter values.

Again, from the curves it is clear that an increment in the number of data produces a performance improvement in terms of estimator bias and/or accuracy. From this results, the effectiveness of the proposed algorithm is evident, and it can be claimed that a good trade-off between the quality of estimate and the computational complexity can be translated in a number of samples equal to $10^5$, that is the value set for all the subsequent tests. This choice is also motivated by the fact that 5G - mmWave (e.g., at 28 GHz with a bandwidth $> 500$ MHz) devices moving at 50 km/h require channel estimation updates every 80 $\mu$s [38]. This latter is guaranteed by the wide available bandwidth, corresponding to more than $80000$ samples which matches with the value assumed in the conducted tests.

The second study case refers to the assessment of the performance of the proposed procedure in terms of both NRMSE and ME as functions of the ratio between the average power of the dominant waves and the average power of the remaining diffuse multipath [5], defined as

$$\kappa = \frac{\mathbb{E}\left[\left|rv_1 e^{j\varphi_1} + rv_2 e^{j\varphi_2}\right|^2\right]}{\mathbb{E}\left[|\varepsilon|^2\right]} = \frac{\mathbb{E}\left[r^2\right]\mathbb{E}\left[v_1^2 + v_2^2\right]}{\sigma^2} = \frac{\Omega\left(v_1^2 + v_2^2\right)}{\sigma^2} = \frac{v_1^2 + v_2^2}{\sigma^2}, \tag{42}$$

where we have exploited the fact that $\Omega = 1$. The considered

simulation setting is the same as the previous scenario[3], viz. $v_1^2 = 5$, $v_2^2 = 4$, and $m = 5$, whereas the total number of data to estimate the sample moments is $N = 10^5$. Figure 4 shows the NRMSE versus parameter $\kappa$ for all the considered estimates, whereas Figure 5 contains the ME with the corresponding confidence interval for each estimate. Again, the true value of the parameter under investigation is indicated with a black dashed curve. The interesting results show that as $\kappa$ grows, the estimation errors and the confidence intervals tend to get smaller and smaller thanks to the increasingly reduced impact of the diffusive component on the received signal.

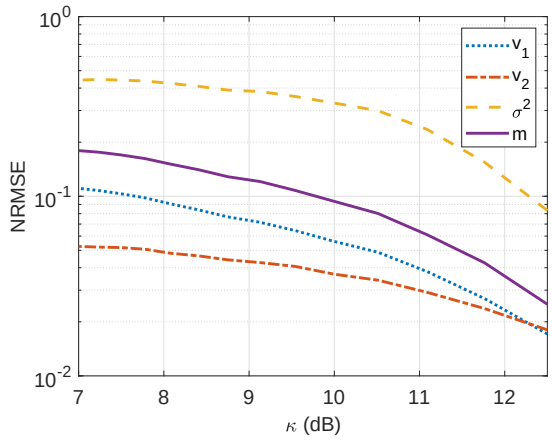


Figure 4. NRMSE versus $\kappa$. The considered simulating scenario assumes $v_1^2 = 5$, $v_2^2 = 4$, $m = 5$, and $N = 10^5$. A total of $M_C = 1000$ Monte Carlo trials are performed.

To corroborate the above results, in the following analysis, the estimation errors are observed with respect to the variation of the ratio between the powers of the two dominant waves, namely

$$\rho_v = \frac{v_2^2}{v_1^2}, \quad \text{with } v_2^2 \leq v_1^2 \tag{43}$$

This analysis is aimed at understanding the behavior of the proposed procedure when the two dominant paths share almost the same power as well as when a strong mismatch among their levels is observed. In fact, herein $\rho_v$ varies from 0 to 1 to characterize the discrepancy between the powers of two dominant LoS waves. Precisely, Figure 6 and Figure 7 report respectively the results associated with this test in terms of NRMSE and ME with respect to $\rho_v$, leaving unaltered the parameter $\kappa$. Note that, the estimation errors are close to 0 for many $\rho_v$ values, except for $\rho_v = 0$ and $\rho_v > 0.8$. As a matter of fact, when $\rho_v = 0$, the residual estimation error is evidently due to the fact that the considered model is based on the assumption that $v_2^2 > 0$ (i.e., $v_2 > 0$). Precisely, when $v_2 = 0$, it is always overestimated since negative values are automatically discarded by the estimation procedure. As a consequence of the fact that $\kappa$ is constant, $v_1^2 + v_2^2$ is also

[3]Note that, the variation of $\kappa$ is realized keeping fixed $v_1^2$ and $v_2^2$ and varying $\sigma^2$.

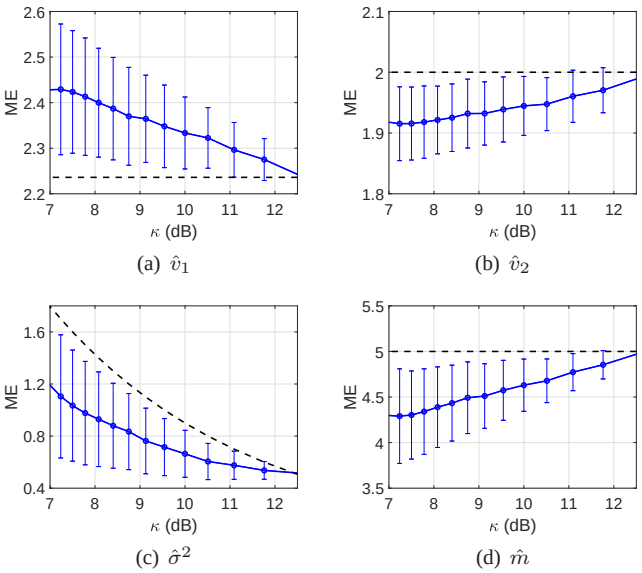


Figure 5. ME with confidence interval versus $\kappa$. The considered simulating scenario assumes $v_1^2 = 5$, $v_2^2 = 4$, $m = 5$, and $N = 10^5$. A total of $M_C = 1000$ Monte Carlo trials are performed. Subplots refers to the estimates a) $\hat{v}_1$, b) $\hat{v}_2$, c) $\hat{\sigma}^2$, and d) $\hat{m}$. Black dashed lines indicate the true parameter values.

constant, and consequently $v_1$ is always underestimated when $\rho_v = 0$. This behavior is perfectly reflected by the results reported in subplots a) and b) of Figure 7. On the other hand, for $\rho_v > 0.8$ it could be observed that when the two dominant waves have approximately the same power levels, some estimation errors could occur, due to the difficulties in discern the two rays.

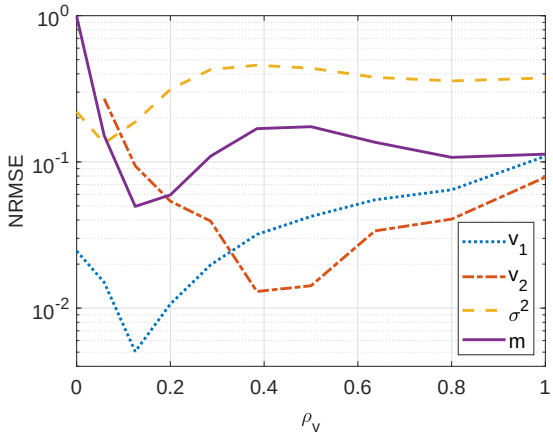


Figure 6. NRMSE versus $\rho_v$. The considered simulating scenario assumes $\sigma^2 = 1$, $m = 5$, $N = 10^5$, and $\kappa = 9$. A total of $M_C = 1000$ Monte Carlo trials are performed.

The next analysis is aimed at testing the robustness of the proposed technique with respect to the variation in the parameter $m$ of the Nakagami distribution. As before, Figures 8 and 9 represent the NRMSE and ME with respect to $m$

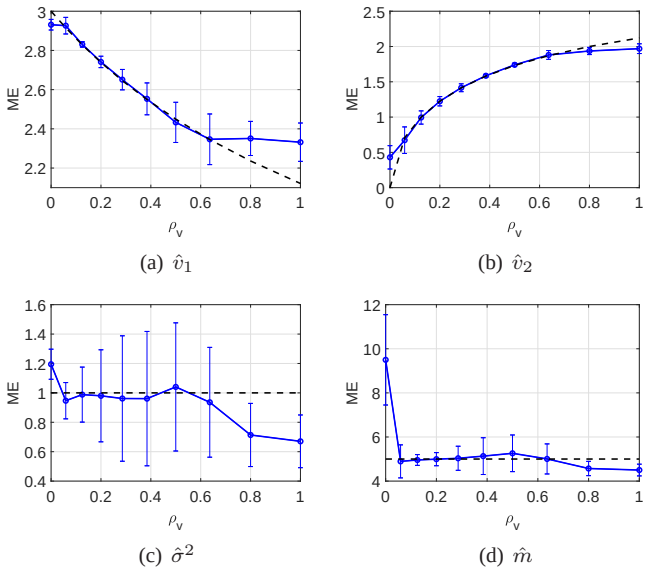


(a) $\hat{v}_1$ (b) $\hat{v}_2$

(c) $\hat{\sigma}^2$ (d) $\hat{m}$

Figure 7. ME with confidence interval versus $\rho_v$. The considered simulating scenario assumes $\sigma^2 = 1$, $m = 5$, $N = 10^5$, and $\kappa = 9$. A total of $M_C = 1000$ Monte Carlo trials are performed. Subplots refers to the estimates a) $\hat{v}_1$, b) $\hat{v}_2$, c) $\hat{\sigma}^2$, and d) $\hat{m}$. Black dashed lines indicate the true parameter values.

for all the considered parameter estimates assuming $v_1^2 = 5$, $v_2^2 = 4$, and $\sigma^2 = 1$. Again, $N = 10^5$ samples data are utilized to obtain the moments estimates. Interestingly, the curves emphasize the capabilities of the proposed procedure to effectively estimate the parameter $v_1$, $v_2$, and $\sigma^2$ in almost all the operating scenarios. Obviously, the errors of $\hat{m}$ increases with respect to $m$. This essentially derives from the fact that the Nakagami random variable can be generated as the square root of the sum of $2m$ squared i.i.d. Gaussian random variables, and consequently the estimate of $m$ becomes more and more difficult when $m$ increases as a consequence of the Central Limit's Theorem.

To conclude the performance assessment on simulated data, the proposed algorithm is compared with the one devised in [32], referred to as Nakagami Based-estimator (NB-E), for the parameter estimates in the presence of Nakagami-$m$ shadowing for the LoS component immersed in a diffusive scenario with no reflected paths for that model. In order to match the signal model of [32], we set $v_2^2 = 0$, $\sigma^2 = 1$, and $m = 5$. The analysis is conducted evaluating the NRMSE for the estimate of $\kappa$ considering $v_1^2 = 5$, and the corresponding result is depicted in Figure 10. The figure emphasizes that both the algorithms are able to estimate the parameter $\kappa$ with low estimation errors when the number of sample data is sufficiently high. However, in general, the NB-E outperforms our algorithm, indicated in the figure as FTR-estimator (FTR-E), which experiences some performance losses due to the mismatch between the nominal and actual data model. We recall that, this scenario corresponds to the above-mentioned case $\rho_v = 0$, where the simulations have shown non zero errors. In fact, its estimation performances do not tend to zero as the number of data

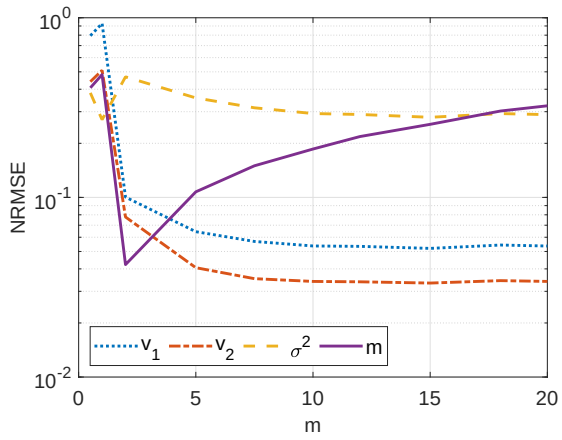


Figure 8. NRMSE versus $m$. The considered simulating scenario assumes $v_1^2 = 5$, $v_2^2 = 4$, $\sigma^2 = 1$, and $N = 10^5$. A total of $M_C = 1000$ Monte Carlo trials are performed.

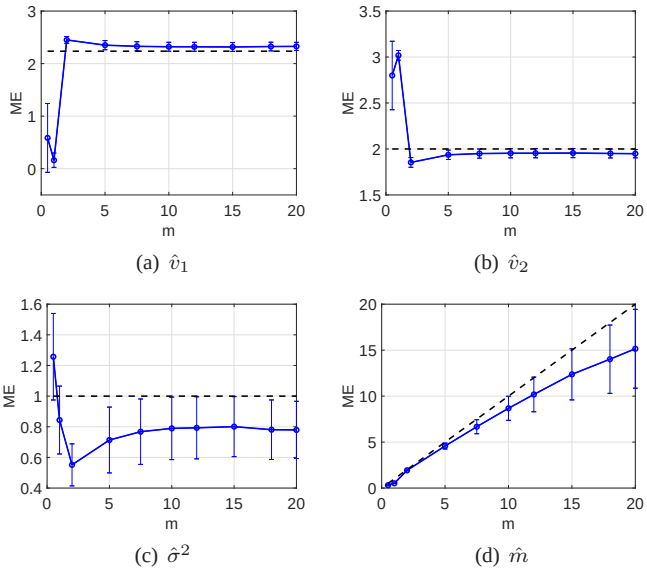


(a) $\hat{v}_1$ (b) $\hat{v}_2$

(c) $\hat{\sigma}^2$ (d) $\hat{m}$

Figure 9. ME with confidence interval versus $m$. The considered simulating scenario assumes $v_1^2 = 5$, $v_2^2 = 4$, $\sigma^2 = 1$, and $N = 10^5$. A total of $M_C = 1000$ Monte Carlo trials are performed. Subplots refers to the estimates of a) $v_1$, b) $v_2$, c) $\sigma^2$, and d) $m$. Black dashed lines indicate the true parameter values.

increase (a floor on the NRMSE is observed) as a consequence of the fact that the FTR-E is actually working in a scenario that does not adhere to its design assumption. It turns out that even though the FTR-E experiences a performance degradation with respect to the NB-E, it can be exploited for much complicated scenarios. In fact, the model considered in this paper is more general, because it is able to estimate a possible reflected ray in addition to the direct one. Such a capability can be particularly useful under vehicular scenarios, where a relevant secondary path may suddenly arise due to mobile equipment's motion. Moreover, it is important to stress here that the NB-E may fail

when applied to a scenario comprising two rays (which does not correspond to its design assumptions). As a matter of fact, in this case, no real solutions[4] come from the straightforward application of the NB-E; this has been also numerically proved through simulations and typically happens when the second ray is not so small to be confused with noise. This behavior can be observed in Figure 11 where the NRMSE of the parameter $v_1$ is plotted as a function of the second ray scaling factor $v_2$. Precisely, the evaluation has been conducted for $v_1^2 = 5$, $N = 10^5$, $\sigma^2 = 1$, and $m = 5$, with $v_2$ taking on values in $[0, v_1]$. As expected, when $v_2$ is close to 0 the NB-E represents the best solution, but as $v_2$ increases, the FTR-E overcomes the former in estimation performance. More importantly, the curve associated with the NB-E is limited to a certain interval because for higher values of $v_2$ the NB-E fails in computing its solutions providing complex values as claimed above. To definitely demonstrate the superiority of the FTR-E over the NB-E, in Figure 12, the NRMSE of the parameter estimates $\hat{v}_1$, $\hat{m}$, and $\hat{\sigma}^2$ is shown versus $N$ for the following simulation setting: $v_1 = \sqrt{5}$, $v_2 = 0.8$,$\sigma^2 = 1$, and $m = 5$. As clearly highlighted by the curves, the FTR-E is able to outperform its competitor in spite of the used number of sample and for each considered parameter under investigation.

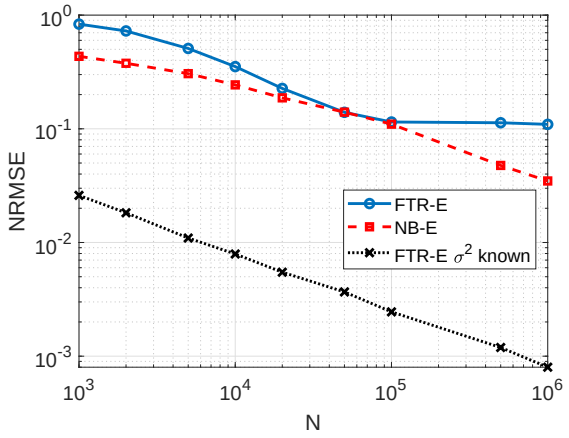


Figure 10. NRMSE of $\hat{\kappa}$ versus $N$ for a one-ray scenario. The considered simulating scenario assumes $v_1^2 = 5$, $v_2^2 = 0$, $\sigma^2 = 1$, and $m = 5$. A total of $M_C = 1000$ Monte Carlo trials are performed.

## B. Measured Data

In this last subsection the proposed algorithm is assessed over measured mmWave data. Precisely, the focus is on the 28 GHz data used in [25]; in [24], the authors show that such data follow the FTR fading model. Figure 13 shows the empirical cumulative density function (ECDF) of the above mentioned data extracted from [25, Fig. 6] and [24, Figs. 8-9]. The two subplots refer to the LoS and NLoS cases, respectively.

[4]The discriminant of the second order equation in (8) of [32] can be negative, even when the true moments are used as starting points in the estimation procedure.

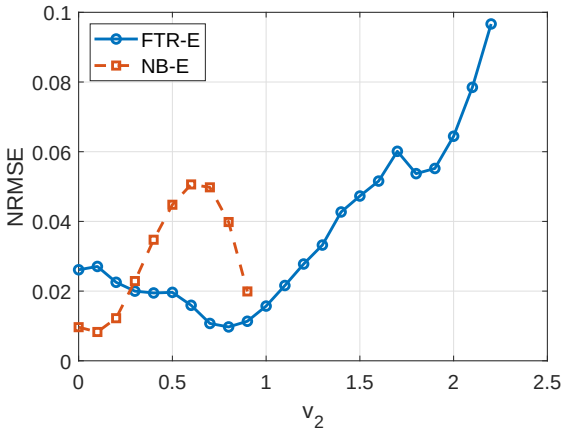


Figure 11. NRMSE of $\hat{v}_1$ versus $v_2$. The considered simulating scenario assumes $v_1^2 = 5$, $N = 10^5$, $\sigma^2 = 1$, and $m = 5$. A total of $M_C = 1000$ Monte Carlo trials are performed.

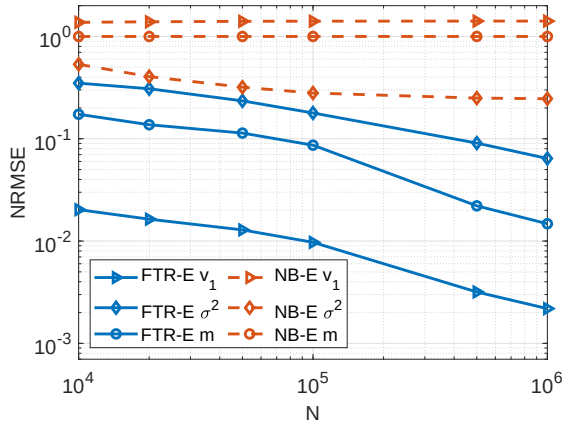


Figure 12. NRMSE versus the number of samples $N$. The considered simulating scenario assumes $v_1 = \sqrt{5}$, $v_2 = 0.8$, $\sigma^2 = 1$, and $m = 5$. A total of $M_C = 1000$ Monte Carlo trials are performed.

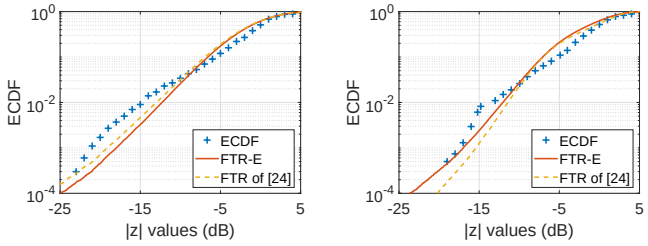


(a) LoS (b) NLoS

Figure 13. ECDFs of the received signal amplitude for LoS and NLoS scenario of measured data obtained from [25, Fig. 6] and [24, Figs. 8-9].

The tests have been conducted running the proposed FTR-E with the four moments computed directly from the available ECDF of the mmWave data. The results of the proposed FTR-E are expressed in terms of $\hat{\kappa}$, $\hat{m}$, and $\hat{\Delta} = 2\hat{v}_1\hat{v}_2/(\hat{v}_1^2 + \hat{v}_2^2)$

and are reported in Table I together with those given in [24]. From the table, it can be observed that the estimated values of the quoted parameters are close to those provided in [24] where the authors have shown that FTR represents a better approximation of data than the one-ray model. As observed from the table, in the challenging NLoS scenario the estimated parameters describing the power contributions, viz., $\kappa$ and $\Delta$, are quite close to those empirically found in [24]. Differently, the estimate of parameter $m$ obtained with the FTR-E is lower than the provided in [24]. To have a better overview of the behavior of the proposed approach, the ECDF taken from [24], together with the theoretical CDFs obtained by the two sets of distribution parameters of the two ray model of Table I, are also plotted in Figure 13. From a visual inspection, it is evident that the two CDFs are almost overlapped for the LoS scenario, whereas in the NLoS case the CDF computed with the parameters obtained from the proposed FTR-E even shows a better match to the measured CDF data for low values of $|z|$, in comparison with the CDF curve computed by the best fitting parameters in [24] also reported in Table I.

Table I. FTR MODEL PARAMETERS PROVIDED IN [24] AND ESTIMATED WITH THE PROPOSED FTR-E.

| | | values from [24] | FTR-E |
|---|---|---|---|
| LoS | $\kappa$ | 80 | 81.0853 |
| | $\Delta$ | 0.5873 | 0.5892 |
| | $m$ | 2 | 2.1816 |
| NLoS | $\kappa$ | 32.7 | 29.6258 |
| | $\Delta$ | 0.8331 | 0.7814 |
| | $m$ | 10 | 4.7206 |

## V. CONCLUSIONS

In this paper the problem of parameter estimation for a FTR model in the context of wireless mobile communications has been considered. Precisely, the received signal has modeled as the sum of two dominant components plus diffusive secondary contributions. The first dominant component is associated with a direct path and the second dominant component arises from a reflection on terrain. In addition, it has also been assumed that the signals of interest are affected by random amplitude shadowing, statistically distributed as Nakagami-$m$, multiplied by unknown scaling factors with random uniform independent phases. Moreover, the diffusive component is assumed to be complex Gaussian distributed.

To estimate the involved parameters, the method of moments has been applied, leading to the derivation of a sophisticated and strongly nonlinear $4 \times 4$ system of equations, whose solution is hard to recover. Therefore, an efficient procedure to solve it has been developed exploiting some a-priori information on the diffusive component power level. The effectiveness of the proposed estimation technique has been shown by evaluating the NRMSEs as well as the MEs and standard deviations in several operating conditions of practical interest. In addition, the proposed procedure has been compared with an existing algorithm developed for the particular case of only one-ray, in a scenario comprising one dominant ray plus a diffusive component. Finally, the proposed technique has been also applied to measured mmWave data to assess its behavior in practical environments confirming what observed on simulated data.

Possible future works might concern additional tests of the proposed algorithm on real recorded data as well as the extension of the proposed framework to more complicated signal models, as for instance an FTR model with different fluctuations experienced by the two rays. Finally, it could be desirable to have a preliminary stage for the estimation of the number of dominant LoS rays which, in principle, would allow to select the best estimator. This study is actually under investigation and will be presented in future works.

## ACKNOWLEDGMENTS

This work was supported in part by the National Science Fund of China under Grant Nos. 61631016 and 61701490.

The authors would like to thank the Editor and the Referees for the interesting questions and comments that have helped to improve this paper.

The authors would also like to thank Prof. Theodore S. Rappaport of the New York University Polytechnic School of Engineering and Dr. F. Javier Lopez-Martinez of University of Malaga for the interesting discussions.

## APPENDIX

### A. Derivation of the Sixth and Eighth Moment of FTR Received Signal

As observed for the second and fourth moment, exploiting the independence among the involved random variables, the sixth and eighth moments of $z$ can be obtained as

$$\begin{aligned}\mu_6 = \mathbb{E}[|z|^6] &= \left[v_1^6 + v_2^6 + 3v_1^4v_2^2 + 3v_1^2v_2^4 + 6(v_1^2+v_2^2)v_1^2v_2^2\right] \\ &\times \frac{(m+1)(m+2)}{m^2} + 6\left(v_1^2+v_2^2\right)\sigma^4 \\ &+ 3\left(v_1^4+v_2^4+2v_1^2v_2^2+2v_1^2v_2^2\right)\sigma^2\frac{m+1}{m} + 6\sigma^6 \\ &+ 12\left(v_1^2+v_2^2\right)\sigma^4 + 6\left(v_1^2+v_2^2\right)^2\sigma^2\frac{m+1}{m} \\ &+ 12v_1^2v_2^2\sigma^2\frac{m+1}{m} \\ &= \left[(v_1^2+v_2^2)^3 + 6(v_1^2+v_2^2)v_1^2v_2^2\right]\frac{(m+1)(m+2)}{m^2} \\ &+ 9\left[(v_1^2+v_2^2)^2 + 2v_1^2v_2^2\right]\sigma^2\frac{m+1}{m} \\ &+ 18(v_1^2+v_2^2)\sigma^4 + 6\sigma^6,\end{aligned} \tag{44}$$

and

$$\begin{aligned}\mu_8 = \mathbb{E}[|z|^8] &= \left[v_1^2+v_2^2+2v_1v_2\cos\left(\varphi_1-\varphi_2\right)\right]^4 \\ &\times \frac{(m+1)(m+2)(m+3)}{m^3} + |\varepsilon|^8 \\ &+ 16\varepsilon_r^4\left(v_1\cos\varphi_1+v_2\cos\varphi_2\right)^4\frac{m+1}{m} \\ &+ 16\varepsilon_i^4\left(v_1\cos\varphi_1+v_2\cos\varphi_2\right)^4\frac{m+1}{m} \\ &+ 6\left[v_1^2+v_2^2+2v_1v_2\cos\left(\varphi_1-\varphi_2\right)\right]^2|\varepsilon|^4\frac{m+1}{m} \\ &+ 24\left[v_1^2+v_2^2+2v_1v_2\cos\left(\varphi_1-\varphi_2\right)\right]^2 \\ &\times \left(v_1\cos\varphi_1+v_2\cos\varphi_2\right)^2\varepsilon_r^2\frac{(m+1)(m+2)}{m^2} \\ &+ 24\left[v_1^2+v_2^2+2v_1v_2\cos\left(\varphi_1-\varphi_2\right)\right]^2 \\ &\times \left(v_1\sin\varphi_1+v_2\sin\varphi_2\right)^2\varepsilon_i^2\frac{(m+1)(m+2)}{m^2} \\ &+ 24\left(v_1\cos\varphi_1+v_2\cos\varphi_2\right)^2\varepsilon_r^2|\varepsilon|^4 \\ &+ 24\left(v_1\sin\varphi_1+v_2\sin\varphi_2\right)^2\varepsilon_i^2|\varepsilon|^4 + 96\varepsilon_r^2\varepsilon_i^2 \\ &\times \left(v_1\cos\varphi_1+v_2\cos\varphi_2\right)^2\left(v_1\sin\varphi_1+v_2\sin\varphi_2\right)^2\frac{m+1}{m} \\ &+ 4\left[v_1^2+v_2^2+2v_1v_2\cos\left(\varphi_1-\varphi_2\right)\right]^3|\varepsilon|^2\frac{(m+1)(m+2)}{m^2} \\ &+ 4\left[v_1^2+v_2^2+2v_1v_2\cos\left(\varphi_1-\varphi_2\right)\right]|\varepsilon|^6 \\ &+ 48\left[v_1^2+v_2^2+2v_1v_2\cos\left(\varphi_1-\varphi_2\right)\right] \\ &\times \left(v_1\cos\varphi_1+v_2\cos\varphi_2\right)^2\varepsilon_r^2|\varepsilon|^2\frac{m+1}{m} \\ &+ 48\left[v_1^2+v_2^2+2v_1v_2\cos\left(\varphi_1-\varphi_2\right)\right] \\ &\times \left(v_1\sin\varphi_1+v_2\sin\varphi_2\right)^2\varepsilon_i^2|\varepsilon|^2\frac{m+1}{m}\end{aligned} \tag{45}$$

or equivalently

$$\begin{aligned}\mu_8 &= \left[(v_1^2+v_2^2)^4+6v_1^4v_2^4+12(v_1^2+v_2^2)^2v_1^2v_2^2\right] \\ &\times \frac{(m+1)(m+2)(m+3)}{m^3} + \left[16(v_1^2+v_2^2)^2+96v_1^2v_2^2\right] \\ &\times (v_1^2+v_2^2)\sigma^2\frac{(m+1)(m+2)}{m^2} \\ &+ \left[72(v_1^2+v_2^2)^2+144v_1^2v_2^2\right]\sigma^4\frac{m+1}{m} \\ &+ 96(v_1^2+v_2^2)\sigma^6+24\sigma^8.\end{aligned} \tag{46}$$

### *B. Probability Density Function of the Two-Ray Model Received Signal*

In this Appendix, the expression of the pdf for the received signal $z$ is provided. Precisely, it is derived resorting to the so-called Law of Total Probability, namely

$$\begin{aligned}&f_z\left(z;\sigma^2,m\right) \\ &= \frac{1}{(2\pi)^2}\int_0^{2\pi}\int_0^{2\pi}\int_0^{+\infty} f_{z|r,\varphi_1,\varphi_2}\left(z;r,\varphi_1,\varphi_2,\sigma^2\right) \\ &\times p_r\left(r;m,1\right)dr\,d\varphi_1\,d\varphi_2,\end{aligned} \tag{47}$$

where $f_{z|r,\varphi_1,\varphi_2}\left(z;r,\varphi_1,\varphi_2,\sigma^2\right)$ is the conditional pdf of the received signal $z$ given $r$, $\varphi_1$, $\varphi_2$, and $\sigma^2$, whereas $p_r\left(r;m,1\right)$ is the pdf of $r$ whose expression is reported in (2).

Now, observe that, given $r$, $\varphi_1$, and $\varphi_2$, $z \sim \mathcal{CN}\left(\left(v_1e^{j\varphi_1}+v_2e^{j\varphi_2}\right)r,\sigma^2\right)$, then (47) can be recast as

$$\begin{aligned}&f_z\left(z;\sigma^2,m\right) \\ &= C\int_0^{2\pi}\int_0^{2\pi}\int_0^{+\infty} r^{\mu-1}\exp\left\{-\beta r^2-\gamma r\right\}dr\,d\varphi_1\,d\varphi_2,\end{aligned} \tag{48}$$

where $C = \left[m^m\exp\left\{-|z|^2/\sigma^2\right\}\right]/\left[2\pi^3\sigma^2\Gamma(m)\right]$, $\beta = \left|v_1e^{j\varphi_1}+v_2e^{j\varphi_2}\right|^2/\sigma^2+m > 0$, $\gamma = \gamma(\varphi_1,\varphi_2) = -2\Re\left\{z\left(v_1e^{-j\varphi_1}+v_2e^{-j\varphi_2}\right)\right\}/\sigma^2$, and $\mu = 2m > 0$.

The integral with respect to $r$ can be solved resorting to [31, Sec. 3.462] to obtain

$$\begin{aligned}f_z\left(z;\sigma^2,m\right) = \int_0^{2\pi}\int_0^{2\pi} &A\exp\left(\frac{\left(\gamma(\varphi_1,\varphi_2)\right)^2}{8\beta}\right) \\ &\times D_{-\mu}\left(\frac{\gamma(\varphi_1,\varphi_2)}{\sqrt{2\beta}}\right)d\varphi_1\,d\varphi_2,\end{aligned} \tag{49}$$

where $A = C(2\beta)^{-\mu/2}\Gamma(\mu)$, and

$$\begin{aligned}D_\mu(\zeta) &= 2^{\mu/2}e^{-\zeta^2/4} \\ &\times \left[\sqrt{\zeta}/\Gamma[(1-\mu)/2]\Phi\left(-\mu/2,1/2;\zeta^2/2\right)\right. \\ &\left.-\sqrt{2\pi}\zeta/\Gamma(-\mu/2)\Phi\left((1-\mu)/2,3/2;\zeta^2/2\right)\right]\end{aligned} \tag{50}$$

is the Parabolic Cylinder Function [31]. Finally, the expression of the pdf of $z$ is

$$\begin{aligned}f_z\left(z;\sigma^2,m\right) &= \frac{m^m\exp\left\{-|z|^2/\sigma^2\right\}}{2\pi^3\sigma^2\Gamma(m)}\Gamma(\mu) \\ &\int_0^{2\pi}\int_0^{2\pi}\exp\left\{\frac{\Re^2\left\{z\left(v_1e^{j\varphi_1}+v_2e^{j\varphi_2}\right)\right\}}{2\sigma^4\left(\frac{\left|v_1e^{j\varphi_1}+v_2e^{j\varphi_2}\right|^2}{\sigma^2}+m\right)}\right\} \\ &\times\left(\frac{2\left|v_1e^{j\varphi_1}+v_2e^{j\varphi_2}\right|^2}{\sigma^2}\right)^{-\mu/2} \\ &\times D_{-2m}\left(-\frac{2\Re\left\{z\left(v_1e^{j\varphi_1}+v_2e^{j\varphi_2}\right)\right\}}{\sigma^2\sqrt{\frac{2\left|v_1e^{j\varphi_1}+v_2e^{j\varphi_2}\right|^2}{\sigma^2}+m}}\right)d\varphi_1\,d\varphi_2,\end{aligned} \tag{51}$$

## REFERENCES


[1] S. Li, L. Da Xu, and S. Zhao, "5G Internet of Things: A Survey," *Journal of Industrial Information Integration*, vol. 10, pp. 1–9, 2018.

[2] M. Nakagami, "The m-Distribution - A General Formula of Intensity Distribution of Rapid Fading," in *Statistical Methods in Radio Wave Propagation*, pp. 3–36. Elsevier, 1960.

[3] X. Chen, S. Liu, J. Lu, P. Fan, and K. B. Letaief, "Smart Channel Sounder for 5G IoT: From Wireless Big Data to Active Communication," *IEEE Access*, vol. 4, pp. 8888–8899, 2016.

[4] F. Boccardi, R. W. Heath, A. Lozano, T. L. Marzetta, and P. Popovski, "Five Disruptive Technology Directions for 5G," *IEEE Communications Magazine*, vol. 52, no. 2, pp. 74–80, February 2014.

[5] J. Zhang, W. Zeng, X. Li, Q. Sun, and K. P. Peppas, "New Results on the Fluctuating Two-Ray Model with Arbitrary Fading Parameters and its Applications," *IEEE Transactions on Vehicular Technology*, vol. 67, no. 3, pp. 2766–2770, 2017.

[6] V. W. S. Wong, R. Schober, D. W. K. Ng, and L.-C. Wang, *Key Technologies for 5G Wireless Systems*, Cambridge university press, 2017.

[7] M. Olyaee, M. Eslami, and J. Haghighat, "Performance of Maximum Ratio Combining of Fluctuating Two-Ray (FTR) mmWave Channels for 5G and Beyond Communications," *Transactions on Emerging Telecommunications Technologies*, p. e3601, 2018.

[8] George R. Maccartney, Theodore S. Rappaport, Mathew K. Samimi, and Shu Sun, "Millimeter-Wave Omnidirectional Path Loss Data for Small Cell 5G Channel Modeling," *IEEE Access*, vol. 3, pp. 1573–1580, 2015.

[9] George R. Maccartney, Theodore S. Rappaport, Shu Sun, and Sijia Deng, "Indoor Office Wideband Millimeter-Wave Propagation Measurements and Channel Models at 28 and 73 GHz for Ultra-Dense 5G Wireless Networks," *IEEE Access*, vol. 3, pp. 2388–2424, 2015.

[10] Z. Pi and F. Khan, "An Introduction to Millimeter-Wave Mobile Broadband Systems," *IEEE Communications Magazine*, vol. 49, no. 6, pp. 101–107, June 2011.

[11] S. Rangan, T. S. Rappaport, and E. Erkip, "Millimeter-Wave Cellular Wireless Networks: Potentials and Challenges," *Proceedings of the IEEE*, vol. 102, no. 3, pp. 366–385, March 2014.

[12] M. R. Akdeniz, Y. Liu, M. K. Samimi, S. Sun, S. Rangan, T. S. Rappaport, and E. Erkip, "Millimeter Wave Channel Modeling and Cellular Capacity Evaluation," *IEEE Journal on Selected Areas in Communications*, vol. 32, no. 6, pp. 1164–1179, June 2014.

[13] T. S. Rappaport, G. R. MacCartney, M. K. Samimi, and S. Sun, "Wideband Millimeter-Wave Propagation Measurements and Channel Models for Future Wireless Communication System Design," *IEEE Transactions on Communications*, vol. 63, no. 9, pp. 3029–3056, September 2015.

[14] J. Huang, C. Wang, R. Feng, J. Sun, W. Zhang, and Y. Yang, "Multi-Frequency mmWave Massive MIMO Channel Measurements and Characterization for 5G Wireless Communication Systems," *IEEE Journal on Selected Areas in Communications*, vol. 35, no. 7, pp. 1591–1605, July 2017.

[15] M. Polese and M. Zorzi, "Impact of Channel Models on the End-to-End Performance of Mmwave Cellular Networks," in *2018 IEEE 19th International Workshop on Signal Processing Advances in Wireless Communications (SPAWC)*, June 2018, pp. 1–5.

[16] A. Abdi, W. C. Lau, M.-S. Alouini, and M. Kaveh, "A New Simple Model for Land Mobile Satellite Channels: First-and Second-Order Statistics," *IEEE Transactions on Wireless Communications*, vol. 2, no. 3, pp. 519–528, 2003.

[17] H.-Y. Shang, Y. Han, and J.-H. Lu, "Statistical Analysis of Rician and Nakagami-m Fading Channel using Multipath Shape Factors," in *2010 Second International Conference on Computational Intelligence and Natural Computing*, September 2010, vol. 1, pp. 398–401.

[18] G. R. Tsouri and D. M. Wagner, "Threshold Constraints on Symmetric Key Extraction from Rician Fading Estimates," *IEEE Transactions on Mobile Computing*, vol. 12, no. 12, pp. 2496–2506, December 2013.

[19] P. J. Crepeau, "Uncoded and Coded Performance of MFSK and DPSK in Nakagami Fading Channels," *IEEE Transactions on Communications*, vol. 40, no. 3, pp. 487–493, March 1992.

[20] M. D. Yacoub, M. V. Barbin, M. S. de Castro, and J. E. Vargas B., "Level Crossing Rate of Nakagami-m Fading Signal: Field Trials and Validation," *Electronics Letters*, vol. 36, no. 4, pp. 355–357, February 2000.

[21] A. M. O. Ribeiro and E. Conforti, "Field Measurements of the Level Crossing Rate in the Nakagami Mobile Channel Environment," in *SBMO/IEEE MTT-S International Conference on Microwave and Optoelectronics, 2005.*, July 2005, pp. 517–520.

[22] Y. Yao, J. Zheng, and Z. Feng, "Small-Scale Variations of Cross-Polar Discrimination in Nakagami-m Fading Channels," *IEEE Communications Letters*, vol. 16, no. 11, pp. 1820–1823, November 2012.

[23] C. Loo, "A Statistical Model for a Land Mobile Satellite Link," *IEEE Transactions on Vehicular Technology*, vol. 34, no. 3, pp. 122–127, August 1985.

[24] J. M. Romero-Jerez, F. J. Lopez-Martinez, J. F. Paris, and A. J. Goldsmith, "The Fluctuating Two-Ray Fading Model: Statistical Characterization and Performance Analysis," *IEEE Transactions on Wireless Communications*, vol. 16, no. 7, pp. 4420–4432, 2017.

[25] M. K. Samimi, G. R. MacCartney, S. Sun, and T. S. Rappaport, "28 GHz Millimeter-Wave Ultrawideband Small-Scale Fading Models in Wireless Channels," in *2016 IEEE 83rd Vehicular Technology Conference (VTC Spring)*. IEEE, 2016, pp. 1–6.

[26] K. P. Peppas, A. Skrivanos, E. Xenos, J. Zhang, I. Kouretas, and S. Chronopoulos, "Effective Capacity of Fluctuating Two-Ray Channels with Arbitrary Fading Parameters," in *2018 IEEE 19th International Workshop on Signal Processing Advances in Wireless Communications (SPAWC)*, June 2018, pp. 1–5.

[27] G. Yang and M. Xiao, "Performance Analysis of Millimeter-Wave Relaying: Impacts of Beamwidth and Self-Interference," *IEEE Transactions on Communications*, vol. 66, no. 2, pp. 589–600, February 2018.

[28] A. Goldsmith, *Wireless Communications*, Cambridge Univ. Press, Cambridge, U.K., 2005.

[29] W. Zeng, J. Zhang, S. Chen, K. P. Peppas, and B. Ai, "Physical Layer Security Over Fluctuating Two-Ray Fading Channels," *IEEE Transactions on Vehicular Technology*, vol. 67, no. 9, pp. 8949–8953, September 2018.

[30] S. Kotz, H. L. Johnson, and C. B. Read, "Encyclopedia of Statistical Sciences," Tech. Rep., 1982.

[31] I. S. Gradshteyn and I. M. Ryzhik, *Table of Integrals, Series, and Products*, Academic press, 2014.

[32] G. Giunta, C. Hao, and D. Orlando, "Estimation of Rician K-Factor in the Presence of Nakagami-$m$ Shadowing for the LoS Component," *IEEE Wireless Communications Letters*, vol. 7, no. 4, pp. 550–553, August 2018.

[33] E. L. Lehmann and G. Casella, *Theory of Point Estimation*, Springer Science & Business Media, 2006.

[34] G. Casella and R. L. Berger, *Statistical Inference*, vol. 2, Duxbury Pacific Grove, CA, 2002.

[35] K. Levenberg, "A Method for the Solution of Certain Non-Linear Problems in Least Squares," *Quarterly of Applied Mathematics*, vol. 2, no. 2, pp. 164–168, 1944.

[36] D. W. Marquardt, "An Algorithm for Least-Squares Estimation of Nonlinear Parameters," *Journal of the Society for Industrial and Applied Mathematics*, vol. 11, no. 2, pp. 431–441, 1963.

[37] P. K. Sen and J. M. Singer, *Large Sample Methods in Statistics: An Introduction with Applications*, Springer US, 1993.

[38] W. Weigel, "5G Applied to Vertical Industry Use Cases - Car, Health, Industry," in *European Conference on Networks and Communications*, Ljubljana, Slovenia, 2018.